## Title

Optical and mass-spectral characterization of mixed-gas flowing atmospheric-pressure afterglow sources



## Authors

Badal, Sunil P
Farnsworth, Paul B
Chan, George C-Y
et al.

## Publication Date

2021-02-01

## DOI

10.1016/j.sab.2020.106043

Peer reviewed

# Optical and Mass-Spectral Characterization of Mixed-Gas Flowing Atmospheric-Pressure Afterglow Sources

Sunil P. Badal[1], Paul B. Farnsworth[2], George C.-Y. Chan[3], Brian T. Molnar[1], Jessica R. Hellinger[1], and Jacob T. Shelley[1,*]

[1]Department of Chemistry and Chemical Biology, Rensselaer Polytechnic Institute, Troy, NY 12180

[2]Department of Chemistry and Biochemistry, Brigham Young University, Provo, UT 84602

[3]Lawrence Berkeley National Laboratory, Berkeley, CA 94720

[*] Corresponding author; 110 8th St., Troy, NY 12180 USA; email: shellj@rpi.edu

**Keywords**: Flowing Atmospheric-Pressure Afterglow; Ambient Desorption/Ionization; Mass Spectrometry; Atmospheric-Pressure Glow Discharge, Emission Spectroscopy

## Abstract

Plasma-based ambient desorption/ionization (ADI) sources for mass spectrometry (MS) often use helium as the primary discharge gas due to the large reaction cross section of excited helium species with atmospheric gases, which ultimately leads to efficient reagent-ion formation. However, some studies have shown mixed-gas plasmas provide unique advantages. For instance, our group showed that a helium-oxygen flowing atmospheric-pressure afterglow (He:$O_2$-FAPA) source yielded enhanced ion signals for small polar analytes, but compounds with aromatic rings underwent chemical modification to produce pyrylium species. Here, it is shown that the addition of $H_2$ to the helium FAPA gas significantly decreased the reagent-ion signals, but analyte-ion signal was not affected to the same degree as reagent ions. In addition, mass spectra obtained with He:$H_2$-FAPA were chemically cleaner with fewer ions stemming from analyte

species and produced less oxidation of analytes. Addition of nitrogen increased the abundance of negative reagent ions (e.g., $NO_2^-$ and $NO_3^-$) which led to the enhanced ion signal for RDX. To better understand these unique advantages of a mixed-gas FAPA, the impact of molecular-gas ($O_2$, $N_2$, or $H_2$) addition on the optical-emission spectra from the discharge was also measured. Spatially resolved emission was obtained from the anode- and negative-glow regions. In general, addition of small fractions (~0.1%) of molecular gases decreased helium and OH emission intensities. Atomic oxygen and hydrogen emission increased with the addition of $O_2$ and $H_2$, respectively. Furthermore, emission characteristics of $N_2$, $N_2^+$, and NO with respect to molecular gas composition on He-FAPA were also measured. Fundamental plasma parameters, such as OH rotational temperature ($T_{rot}$), were also calculated for these mixed-gas systems.

## 1. Introduction

Ambient desorption/ionization-mass spectrometry (ADI-MS) provides the capabilities to directly desorb/ionize analytes from sample surface in the open air with little or no sample pretreatment, which significantly increases the sample throughput [1]. Since its introduction in 2004 by Takats *et al.* [2], ADI-MS has found many applications ranging from rapid screening of pharmaceutical products [3], explosives [4], and drugs-of-abuse [5], to quantitative analysis [6] and mass-spectral imaging [7-9]. A variety of different ADI-MS sources have been reported with the most extensively used being desorption electrospray ionization (DESI) [2] and direct analysis in real time (DART) [10]. Out of more than 40 ADI-MS sources, at least one third of the techniques are plasma-based [11, 12], which means they rely on electrical discharges for the desorption and/or ionization process. The most widely used plasma-based sources include DART [4, 10, 13, 14], dielectric-barrier discharge ionization (DBDI) [15], low-temperature plasma (LTP) probe [16], flowing atmospheric-pressure afterglow (FAPA) [17-21], atmospheric-

pressure solid analysis probe [22-26], and plasma-assisted desorption/ionization (PADI) [27]. Although, these plasma-based sources have different designs and powering schemes, which leads to very different plasma processes, it has been frequently noted they produce similar reagent and analyte ions in molecular MS.

Plasma-based ADI sources for MS generally use helium as the discharge gas due to the large reaction cross section of excited helium species with atmospheric gases such as $N_2$, $O_2$, $H_2O$, *etc.*, which ultimately leads to greater reagent-ion densities. However, some mixed-gas plasmas were found to provide improved sensitivity compared to only-helium discharges. For instance, Brewer *et al.* [28] showed that the addition of a small percentage of $O_2$ to a He or Ar radiofrequency atmospheric-pressure glow discharge (rf-APGD) enhanced ion signal for some pharmaceutical compounds up to nine times. In addition, mass spectra obtained with this mixed-gas plasma contained fragmentation patterns that were similar to electron-ionization (EI) mass spectra that are database searchable. In another case, Wright *et al.* [29] examined the addition of hydrogen to a helium dielectric barrier discharge (DBD), which led to enhanced ion signals of up to 68 times for several analytes. Further, these signal enhancements were noted for gaseous analytes and analytes coated on glass slides with addition of $H_2$ to an argon plasma.

Here, we explore the effects of molecular gases on the performance and characteristics of the discharge of a helium FAPA source. The FAPA utilizes a direct-current atmospheric-pressure glow discharge (APGD), which is in contrast to the previously reported mixed-gas experiments that used alternating-current (AC) discharges. Molecular gases such as $O_2$, $N_2$, and $H_2$ were added to the He plasma of the FAPA source, while reagent- and analyte-ion signals were measured with mass spectrometry. To better understand the plasma processes and

ionization chemistry, optical emission spectra of mixed-gas plasma of the FAPA source were also recorded.

The use of optical emission spectroscopy (OES) has been used by a number of groups to monitor and understand plasma-based ADI processes. For instance, Chan et al. [30] used spatially resolved OES from the AC dielectric-barrier discharge of a helium LTP to determine the origin of contaminant species, such as $O_2$, $N_2$, and $H_2O$. Franzke et al. [31-34] have measured OES from helium DBDI to better understand plasma processes in the homogeneous and filamentary modes. Shelley et al. [35] applied a combination of OES and MS to characterize differences between the corona-to-glow discharge and the APGD of the DART and FAPA sources, respectively. Similarly, Kratzer et al.[36] compared AC DBD, RF APGD, and the DC DART sources with MS and OES for the direct determination of acetaminophen.

The use of OES also allows determination of fundamental plasma parameters, such as rotational temperature ($T_{rot}$) from OH and $N_2$ emission bands and electron number density ($n_e$) from Stark broadening of the $H_\beta$ line. Chan et al. [37] used spatially resolved rotational temperatures calculated from OH and $N_2$ to elucidate that $He_2^+$ serves as an important energy carrier from the AC LTP discharge to the open air. A similar behavior was observed in the afterglow of a DC helium FAPA source [38]. In that same work, both $T_{rot}$ and $n_e$ were determined at multiple locations within the discharge with maxima in the negative-glow region of 1,170 K and *ca.* $10^{13}$ $cm^{-1}$, respectively.

There have been far fewer optical studies of mixed-gas ADI plasma sources. Schütz et al. [39] presented a survey emission spectrum from an argon-propane DBDI source that, ultimately, was shown to produce similar analyte ions and analytical performance to a helium

DBD. Farnsworth et al. [29, 40, 41] has used a combination of emission, fluorescence, and absorption spectroscopies to monitor changes in helium species, particularly helium metastable atoms ($He^m$), in helium and He:$H_2$ DBD source. We draw on these earlier works to better understand plasma processes occurring in the mixed-gas FAPA sources tested here.

## 2. Experimental

### 2.1. Reagents

All reagents used were analytical grade. Ultra-high purity (UHP) helium (99.999%) and nitrogen (99.999%) were purchased from Airgas (Radnor, PA, USA). This grade of helium has maximum impurity levels of 1 $ppm_v$ $O_2$, 1 $ppm_v$ $H_2O$, 0.5 $ppm_v$ total hydrocarbons, and 5 $ppm_v$ $N_2$. All gas lines were purged for at least an hour before use to minimize impurities beyond those from the main supply. It is important to note that the level of impurities in the gas supply (<5 $ppm_v$) is negligible compared to the amounts of molecular gases added in these studies (>1,000 $ppm_v$); for the sake of simplicity, we ignore molecular gas contributions from impurities in the main helium supply for the comparisons presented below.

Helium/oxygen (80%/20%) and helium/hydrogen (60%/40%) mixtures were also obtained from Airgas (Radnor, PA, USA). Naphthalene, anthracene, benzene, aniline, and RDX (as 1000 µg/mL standard in methanol) were purchased from Sigma-Aldrich (St. Louis, MO, USA). These target compounds were selected for this study to cover a diverse range of analyte properties known to be important in desorption and ionization pathways with plasma-based ADI sources. For instance, aniline was chosen as a species that typically undergoes proton-transfer ionization with protonated water clusters ($[(H_2O)_nH]^+$) to form $MH^+$. Meanwhile, the non-polar character of naphthalene leads to ionization via either charge transfer (with *e.g.*, $O_2^+$, $N_2^+$, or $NO^+$) or photoionization, which yields $M^+$ ions. While anthracene is also non-polar, it has a

sufficiently high proton affinity (877 kJ/mol)[42] to be ionized through proton transfer in addition to charge-transfer or photo ionization. While the aforementioned test species readily form positive ions, RDX typically produces negative ions formed through anion attachment with *e.g.*, $NO_2^-$, $NO_3^-$, or $Cl^-$ (if a source of chloride is present) [10, 16]. Subjecting these species to mixed-gas FAPA conditions allowed for monitoring any changes in ionization pathways.

### 2.2. FAPA Source

A pin-to-plate FAPA source used for these experiments has been described elsewhere [43, 44]. Briefly, a DC atmospheric-pressure glow discharge (APGD) was sustained between a stainless-steel pin cathode (1 mm diameter) and brass plate anode, which were held in place inside a quartz discharge chamber with flowing helium. Discharge species (*e.g.* excited species, ions, and electrons) exited a 1.6-mm hole in the plate where they interact with atmospheric gases and analytes. A high DC potential (*ca.* –500 V) was applied to the pin cathode from a custom built high-voltage power supply (Prosolia Inc., Indianapolis, IN, USA) while the plate anode was connected to ground potential. The FAPA source was powered in current-controlled mode at 20 mA. Helium flow to the source was controlled by a mass flow controller (model C50L-AL-DD-2-PV2-V0-SCR; Sierra Instruments Inc., Monterey, Ca, USA) that can provide a maximum of 5 L $min^{-1}$. Another mass flow controller (model C50L-AL-DD-2-PV2-V0-SCR; Sierra Instruments Inc., Monterey, Ca, USA) that can provide up to 25 mL/min was used to control $He/O_2$, $He/H_2$, or nitrogen flow, which was mixed with the main helium flow in a T-junction just before the discharge chamber. These mass flow controllers have a repeatability of ±0.25% of full the scale, which equates to ±13 mL/min and ±0.063 mL/min for the main helium flow and the supplemental molecular-gas flow, respectively. In this setup, these two flow controllers and the

aforementioned mixed-gas supplies result in maximum molecular gas compositions of 0.5% $O_2$, 1.0% $H_2$, or 2.5% $N_2$.

As can be seen in Figure S4, the FAPA discharge power increased monotonically with $O_2$ and $N_2$ composition. Oxygen addition led to a greater change in discharge power with an increase of 25% when 0.5% $O_2$ was added to the discharge, compared to an 18% power increase for the same amount of $N_2$ in the discharge. Interestingly, addition of $H_2$ to the helium FAPA required lower voltages and powers to sustain the discharge. As $H_2$ composition was elevated above 0.3%, the discharge voltage and power began to rise. The biggest change in discharge power for $H_2$ addition, compared to only helium, was -10% at an $H_2$ composition of 0.3%.

A manual translational stage (PT3; Thorlabs Inc., Newton, NJ, USA) was used to precisely align the FAPA source with the mass spectrometer inlet. Volatile analytes were introduced to the FAPA afterglow through a fused-silica capillary with helium as the carrier gas at 10 mL/min flow rate. Solid analytes were introduced to the FAPA afterglow with a glass probe fixed on a one-dimensional translational stage (PT1; Thorlabs Inc., Newton, NJ, USA), similar to the methods described before [18, 19].

Higher resolution optical emission spectra of mixed-gas FAPA sources, which were performed at Brigham Young University, used a different flow mixing setup. For the He:$H_2$ and He:$O_2$ mixtures, the flows from two sources, UHP He (99.999% purity) and 1% $H_2$ or $O_2$ in He, were combined using two matched mass flow controllers (MKS model 1170A, Andover, MA). The flows from the two sources were varied to give a final support gas ranging from UHP He (containing a maximum of 0.0005% v/v molecular gas impurity) to 1% of the dopant gas in He, at a total flow rate of 1 L $min^{-1}$. For the He-$N_2$ mixture, low flows of pure $N_2$ gas were metered

into a flow of UHP He to give the desired $N_2$ percentages. The $N_2$ flows were delivered by a mass flow controller (Teledyne Model HFC-302, Thousand Oaks, CA) that had been calibrated with a primary calibrator (Definer 220, Mesalabs, Butler, NJ) to ensure accurate final concentrations of added $N_2$ to be between 0% and 1%, though it should be noted that the UHP He supply contained $N_2$ at a maximum impurity level of 5 $ppm_v$.

### 2.3. Mass Spectrometry

Mass spectra were acquired with a Thermo LTQ XL linear ion trap mass spectrometer (Thermo Scientific, San Jose, CA, USA). The LTQ-XL mass spectra were collected with a maximum injection time of 100 ms, three microscans per spectrum, and a capillary temperature of 275 °C. Capillary and tube-lens voltages of 15 and 65 V, respectively, were used to detect larger-mass analyte ions. To acquire reagent-ion mass spectra in the positive-ionization mode, the instrument was operated in the low mass range mode, which allows detection of ions down to *m/z* 15. In this mode, the capillary and tube lens voltages were decreased to 2 and 31 V, respectively.

Any changes in reagent- or analyte-ion signals from a He-FAPA to a mixed-gas FAPA are reported as relative signal differences. Additionally, it is well known that the background level and structure (i.e. background ions formed/detected) in ADI-MS varies across instrument type, local environment, sample probe/substrate used, etc. Therefore, any reported changes in analyte-ion signal were background subtracted prior to taking the ratio. These studies were conducted to broadly characterize shifts in molecular ionization and plasma processes with different mixed-gas FAPA systems; a more detailed examination of S/N or S/B changes with mixed-gas FAPA should be carried out for a particular application where analytes and required limits-of-detection are well defined.

### 2.4. Emission Spectroscopy

Optical emission spectra were recorded in two locations with two different spectrometers. In one case, a fiber-coupled Avantes six channel spectrometer (Model: AVS-RACKMOUNT-USB2, Avantes Inc., Apeldoorn, Netherlands) capable of simultaneously measuring emission from 175 to 1100 nm was used to measure low-spectral resolution (*ca.* 0.1 nm) emission profiles from the FAPA source. Using this setup for inspecting the mixed-gas FAPA sources allowed emission to be collected from a spot of only *ca.* 50 µm in diameter. Translation of the FAPA under the collection optics enabled collection of spatially resolved emission. Emission spectra from the negative glow and the anode glow of the FAPA operated with helium, He:$O_2$, He:$H_2$, and He:$N_2$ can be found in Figures S1-S3 of the Supplemental Information.

Higher-resolution optical spectra were obtained to determine rotational temperatures within the plasmas. For these measurements, the plasma was imaged onto the entrance slit of a monochromator (model 2061, McPherson, Chelmsford, MA) with unit magnification. Matched achromats were used for collection of the $N_2^+$ spectra, and matched plano-convex fused-silica lenses were used to collect the $N_2$ and OH spectra. In the latter case, the positions of the lenses were adjusted to compensate for chromatic aberration at the UV wavelengths. The entrance slit of the monochromator was 2 mm high and 20 µm wide. Because the negative glow was a thin layer very near the tip of the stainless-steel pin cathode, the discharge was positioned such that the upper 2 mm of the cathode was in the viewing region during collection from the negative glow. For collection of emission from the anode glow, the discharge was lowered by 7 mm, resulting in collection of radiation from the region immediately below the brass cap that served as the anode.

High-resolution spectra were obtained with a 1200 groove/mm grating installed on the 1-meter monochromator, which, combined with the 20-μm entrance and exit slits, produced a nominal instrumental linewidth of 17 pm. Given the stigmatic optics of the monochromator and the relatively small slit height, the actual instrumental width is close to the nominal value. Radiation emerging from the exit slit of the monochromator impinged on a photomultiplier tube (R928, Hamamatsu, Hamamatsu City, Japan), and the resulting photocurrent was converted to a voltage with a commercial amplifier (Keithley, model 428, Beaverton, OR). Voltages were then digitized and stored for further analysis.

### 2.5. OH rotational temperature determination

The method used here to calculate rotational temperature is same as explained by Chan *et al.* [45] and Shelley *et al*. [43] Briefly, four emission lines in the $Q_1$ branch were used to construct a plot of $\ln(I\lambda/gA)$ versus $E_{exc}$, where $\lambda$, I, $A$, g, and $E_{exc}$ are the emission wavelength, intensity of the line, the transition probability, the degeneracy of the excited energy level, and the energy of the excited state in eV, respectively [43, 45]. The slope of the linear plot obtained was equal to $(-1/kT_{rot})$, where k is the Boltzmann constant in eV $K^{-1}$ and $T_{rot}$ is the rotational temperature in K [43, 45]. The relative slope error was used to calculate the relative standard deviation of calculated temperatures [43].

## 3. Result and discussion

### 3.1. **He:$O_2$-FAPA source for mass spectrometry**

Significant presence of molecular gases in the atomic plasmas (e.g., He, Ar, etc.) often quench reagent-ion formation, which results in little or no analyte signals. Therefore, most plasma-based ADI sources are operated with ultra-high purity gases; even then, ultra-high purity

helium (99.999%) contains small amounts of water (< 0.5 ppm) and other impurities. In addition, water molecules adsorbed on the inner wall of transfer lines gets swept into the discharge. It has been shown that these impurities can be effectively removed before the discharge chamber, but only with rather cumbersome approaches[46].

In this study, small fractions of molecular gases were controllably added to the helium glow discharge of a FAPA source to study the effects on plasma processes and ionization chemistries. Previously, our group has shown that the addition of a small fraction (0.1%, v/v) of $O_2$ enhances the protonated water cluster signal with corresponding enhancement in ion signals for small, polar analytes like acetone and methanol [44]. In contrast, compounds with aromatic rings undergo chemical modification in the He:$O_2$-FAPA to produce pyrylium ions (*e.g.*, $[M-3H+O]^+$). Formation of pyrylium was confirmed with the help of exact mass measurement, tandem mass spectrometry, measurement of isotopically labelled species, and reaction of pyrylium ions formed in the FAPA afterglow with ammonia.

### 3.2. He:$H_2$-FAPA source for mass spectrometry

The effect of addition of molecular hydrogen gas ($H_2$) to He-FAPA was also studied. It was found that the addition of even a small amount of $H_2$ (0.17%, v/v) significantly quenched reagent-ion formation in the FAPA afterglow (*cf.* Figure 1). Specifically, signal for protonated water dimer (*i.e.* $[(H_2O)_2H]^+$) at *m/z* 37 decreased by more than three orders of magnitude. This decline in reagent ions is likely due to the quenching of excited helium atoms by collision with hydrogen molecules, effectively inhibiting the most common reagent-ion formation pathways in helium plasma sources [17, 29, 41]. Similar results were also observed by Heywood *et al.* [41] where collisionally assisted laser-induced fluorescence (LIF) was used to map helium metastable densities in the afterglow of a helium DBD. In the presence of 1% $H_2$, helium metastable atoms

could not be detected in the afterglow plasma of the DBD. In spite of the disappearance of helium metastable atoms and reagent ions, enhanced ion signal was observed for a range of organic analytes [29].

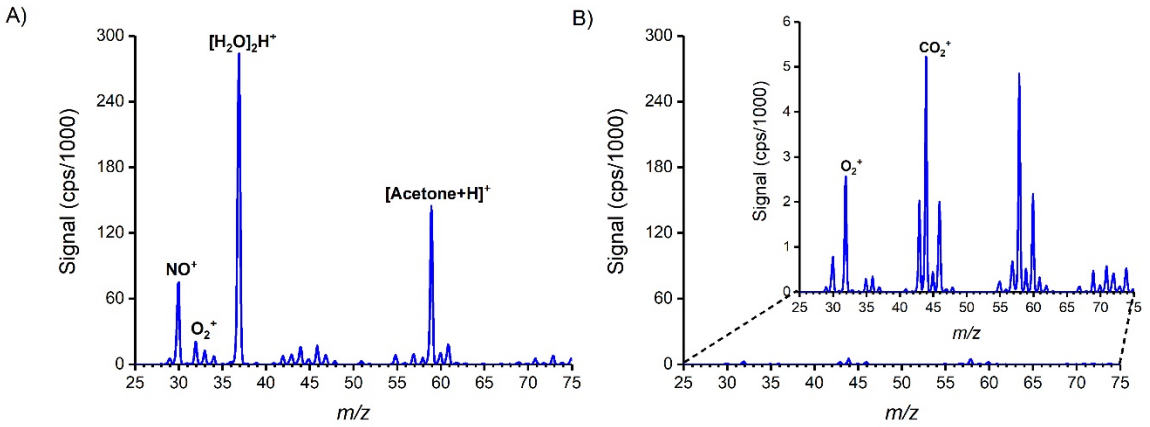


**Figure 1.** Reagent-ion mass spectra obtained with A) He-FAPA and B) He:$H_2$-FAPA with 0.17% v/v $H_2$ (inset shows the zoomed in view of y-axis). Protonated acetone ion signal was due to the presence of acetone in ambient laboratory air.

In the case of the DC FAPA, though, introduction of $H_2$ to the helium discharge of FAPA led to a decrease in analyte-ion signal. Interestingly, though, analyte signal did not decrease to the same degree as that of the reagent ions. As can be seen in the Figure 1B, reagent-ion signal dropped by about two order of magnitude with $H_2$ addition, while aniline, naphthalene and anthracene ion signals decreased only by 3.1, 6.4, and 12.0 times, respectively (*cf.* Figure 2, Figure 3, Figure 4). This disproportionate change indicates that the He:$H_2$ system likely yielded a reagent species that could not be detected via mass spectrometry (e.g., below the low-mass cut-off of the instrument).

Another notable observation with the addition of $H_2$ to FAPA was that there was a noticeable shift in the ionization pathway of analytes with He:$H_2$-FAPA compared to He-FAPA. For aniline, the protonated molecular ion ($MH^+$) was the only species detected with a He:$H_2$-FAPA, while He-FAPA yielded a molecular ion ($M^{+\cdot}$) at 30% of the abundance of $MH^+$ (*cf.* Figure 2). In another case, the molecular cation of naphthalene dominated the mass spectrum

when a He:$H_2$-FAPA was used, while $MH^+$ was the base peak (with $M^{+\cdot}$ at 50% abundance) with He-FAPA (*cf.* Figure 3). Mass spectra of anthracene obtained with He:$H_2$-FAPA was dominated by $MH^+$ with a small amount of $M^{+\cdot}$; these detected species also differ from the mass spectra obtained with He-FAPA (*cf.* Figure 4). In all cases, oxidation of aromatic analytes, a common occurrence in FAPA-MS [19, 20, 47], was significantly lower for a He:$H_2$-FAPA. Overall, a He:$H_2$-FAPA produced chemically cleaner mass spectra albeit with lower total ion signal and fewer analyte ion types.

The shift in ionization pathways and resulting analyte ions combined with the drastic decrease in measured reagent-ion signals indicates formation of alternative reagents or reactive species that cannot be detected with mass spectrometry. As was proposed by Wright et al. [29], some examples of possible reagent species could include $HeH^+$, $H_3^+$, or even high-energy photons [29, 41]. Both $HeH^+$ and $H_3^+$, at *m/z* 5 and 3, respectively, are too low of mass to be detected by the MS instruments used here or by Farnsworth *et al.* [29, 40, 41]. Meanwhile, the role and contribution of vacuum-ultraviolet photoionization with mixed-gas FAPA will be the focus of a future publication. However, preliminary photoionization studies indicate that high-energy photons are not responsible for the shift in ionization pathway [48].

Not surprisingly, naphthalene has a lower proton affinity than anthracene and aniline (803 kJ/mol vs. 877 kJ/mol and 883 kJ/mol, respectively).[42] That would indicate that the reagent responsible for protonating aniline and anthracene (but not naphthalene) has a proton affinity between that of naphthalene and anthracene. The reagent-ion spectra of He:$H_2$-FAPA (*cf.* Figure 1B) did not reveal any protonating reagents of abundance within the mass range that could be recorded. Additionally, the $HeH^+$ and $H_3^+$ reagent ions proposed by Wright et al.[29] might not be the cause of this disparity because both have proton affinities lower than all the

tested analytes by at least 380 kJ/mol.[42] They could not be ruled out entirely, though, because that large of a proton-affinity difference between reagent and analyte can lead to significant fragmentation of analyte ions beyond the mass range recorded in these studies.[49, 50]

Interestingly, acetone, which was detected only in the He-FAPA reagent-ion spectrum (as $MH^+$), has a proton affinity of 812 kJ/mol,[42] so it could protonate aniline and anthracene, but not naphthalene. The lack of protonated acetone signal in the He:$H_2$-FAPA reagent-ion spectrum, though, raises questions about the likelihood of ambient acetone serving as the protonating reagent. In any case, the shift in ionization pathways observed with He:$H_2$-FAPA is unique enough to delve deeper into this in a follow-up study.

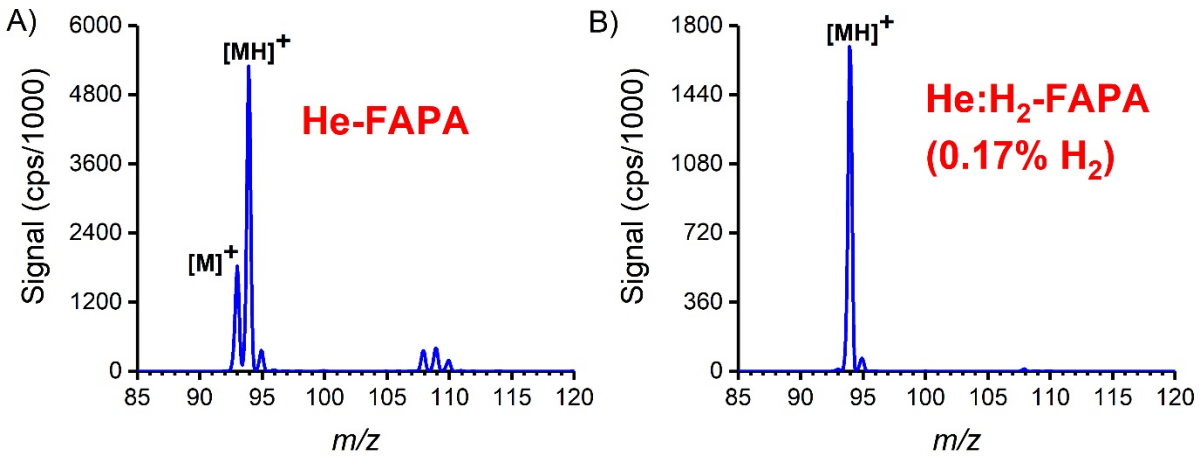


**Figure 2.** Mass spectra of aniline ($C_6H_5NH_2$, M = 93 u) obtained with A) He-FAPA and B) He:$H_2$-FAPA with 0.17% v/v $H_2$.

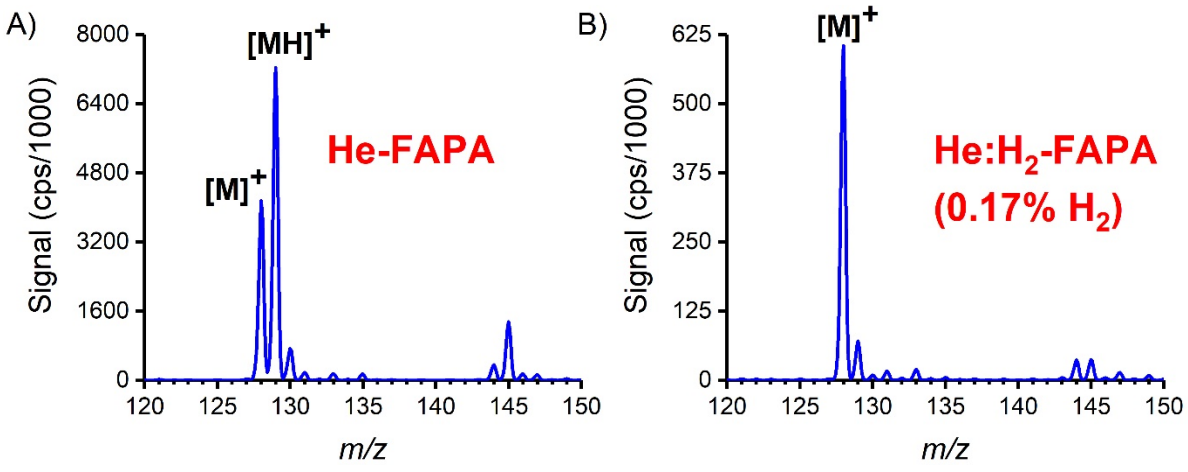


**Figure 3.** Mass spectra of naphthalene ($C_{10}H_{10}$, M = 128 u) obtained with A) He-FAPA and B) He:$H_2$-FAPA (0.17% $H_2$).

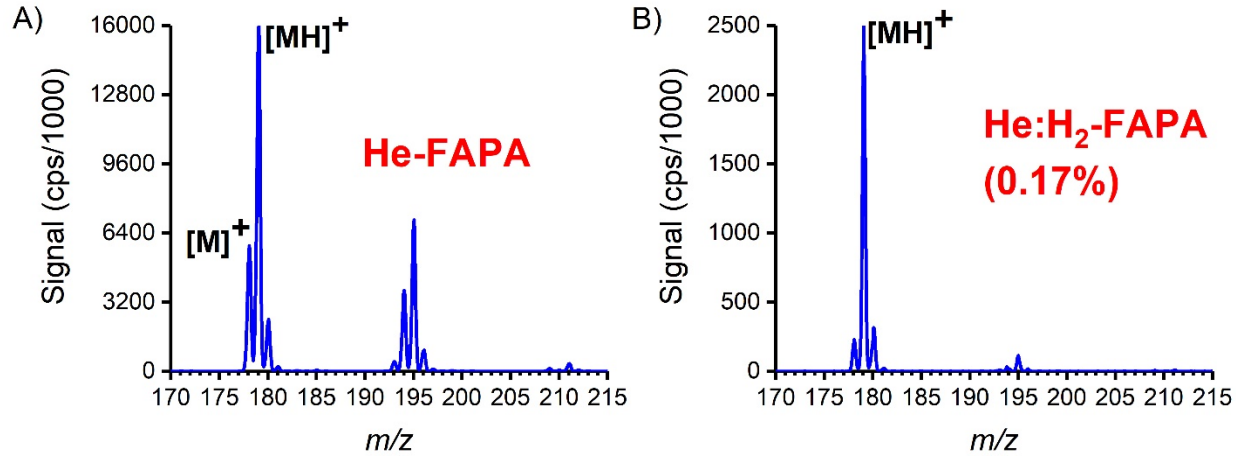


**Figure 4.** Mass spectra of anthracene ($C_{14}H_{10}$, M = 178 u) obtained with A) He-FAPA and B) He:$H_2$-FAPA (0.17% $H_2$).

### 3.3. He:$N_2$-FAPA source for mass spectrometry

For plasma-based ADI-MS sources, $N_2$ plays an important role in afterglow chemistry and reagent-ion formation [17, 51]. To monitor the effect of $N_2$ gas on plasma processes and ionization chemistry within the FAPA source, small fractions of $N_2$ were precisely introduced to the He plasma. In the positive-ionization mode, presence of $N_2$ in the He-FAPA quenched reagent-ion signal, which led to lower analyte signals, similar to $H_2$ addition. In negative-ionization mode, however, reagent-ion signals for $NO_2^-$ and $NO_3^-$ increased with the addition of

0.2% $N_2$ (*cf.* Figure 5). Furthermore, the ratio of $NO_3^-$ to $NO_2^-$ increased from 2.3 to 177.2 with 0.2% $N_2$ in a He-FAPA.

Interestingly, ion signal for the high-explosive RDX significantly increased with He:$N_2$-FAPA compared to He-FAPA. In plasma-based ADI, RDX and other nitrated compounds are typically ionized via anion attachment with $NO_2^-$ and $NO_3^-$ [16, 19]. The $[RDX+NO_3]^-$ signal increased by more than seven times with addition of 0.2% $N_2$, while $[RDX+NO_2]^-$ signal remained nearly the same in the presence of He:$N_2$-FAPA (*cf.* Figure 6). Overall, He:$N_2$-FAPA mass spectra for RDX produced better ion signal and were simpler.

This relative change in analyte-ion abundance was not as drastic as the shift in the ratio of $NO_3^-$ to $NO_2^-$ from the reagent-ion spectra. A number of factors could possibly contribute to this effect including the thermodynamics of the respective anion-attachment reactions (which has not been well characterized) and concentration of $NO_3^-$, $NO_2^-$, and neutral RDX in the ionization region. Further complicating matters, RDX is known to partially dissociate at elevated temperatures to produce $NO_x$ [52], which can be converted to $NO_2^-$ and $NO_3^-$ in plasmas. However, Harper *et al.* [16] reported mass spectra for RDX with an LTP source using helium or air as the discharge gas. They showed that mass spectra obtained with a helium LTP contained $[RDX+NO_2]^-$ at 40% of $[RDX+NO_3]^-$, whereas an air-based LTP yielded $[RDX+NO_2]^-$ that was only 5% of the $[RDX+NO_3]^-$ signal. Though LTP is a different plasma source entirely, their results closely align with the findings of this study and indicate that this phenomenon is common amongst many, or perhaps all, plasma-based ADI-MS sources. From these reports it is clear that $N_2$-doped plasma sources enhance sensitivity and signal-to-noise (S/N), while producing simpler spectra, for the detection of explosives, especially those that ionize via anion attachment (e.g., RDX and HMX).

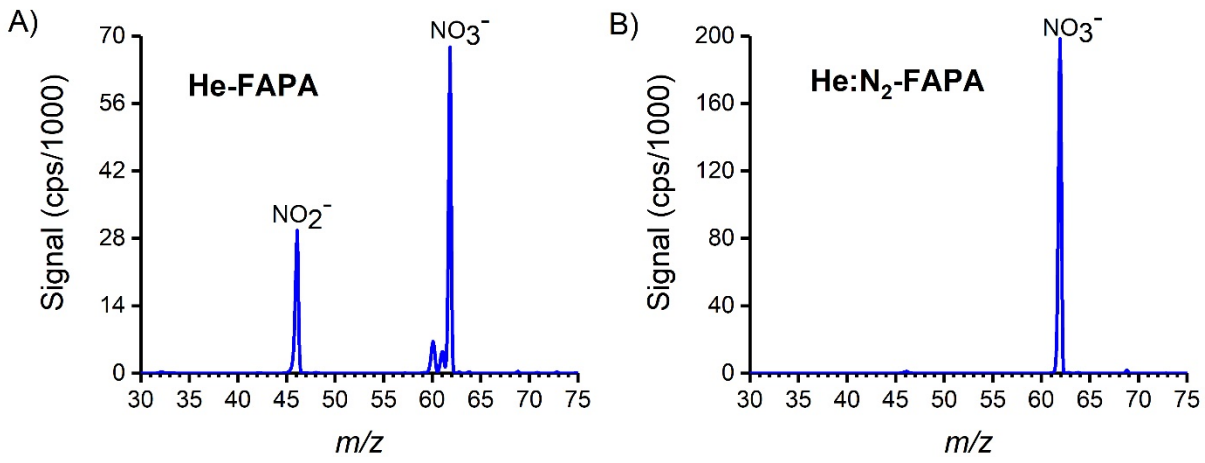


**Figure 5.** Reagent ion mass spectra in negative-ionization mode obtained with A) He-FAPA and B) He-$N_2$-FAPA with 0.2% $N_2$.

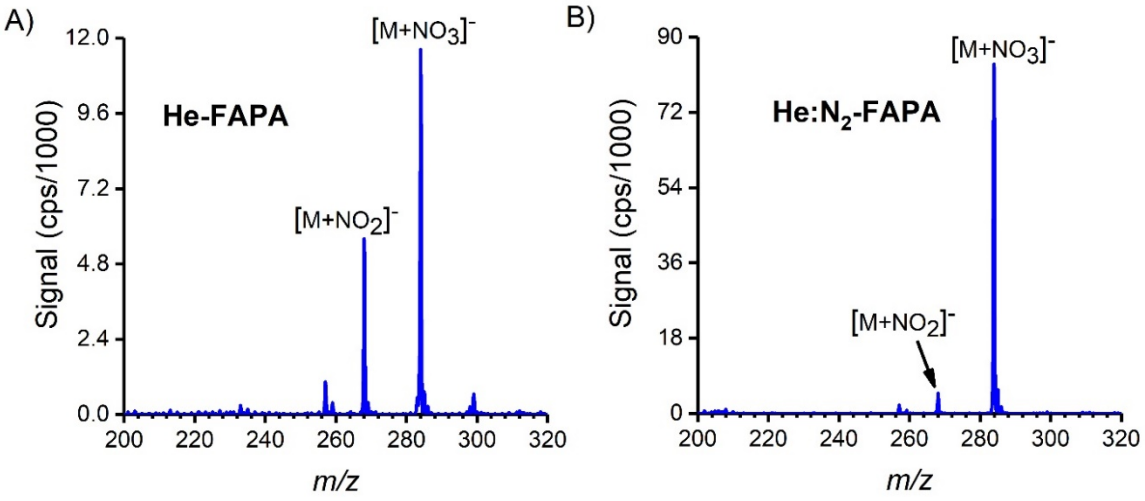


**Figure 6.** Mass spectra of RDX ($C_3H_6N_6O_6$, M = 222 u) in negative-ionization mode obtained with A) He-FAPA and B) He:$N_2$-FAPA with 0.2% $N_2$.

### 3.4. Optical characterization of He:$O_2$-FAPA

Mass-spectral data provides limited information on plasma processes and ionization chemistry and lacks the information on neutral, excited atoms and molecules that might play significant roles in desorption/ionization chemistry. To better understand the ionization

chemistry and plasma processes with mixed-gas FAPA, optical emission from excited species within the discharge was measured. Emission spectra obtained from a He:$O_2$-FAPA discharge showed that addition of $O_2$ decreases emission for most species, including He, $N_2^+$, $N_2$, and OH, whereas atomic oxygen emission (at 777.3 nm) at the anode glow increased with $O_2$ addition up to 0.3% $O_2$ and decreased upon further $O_2$ addition. The decrease in He emission could be explained by quenching of excited He atoms by molecular oxygen.

At the negative glow (i.e. near the cathode), emission from every species except atomic oxygen dramatically decreased with the addition of only 0.1% $O_2$ (*cf.* Figure 7b). Interestingly, though, both He and $N_2$ emission intensity increased monotonically from that point with addition of more $O_2$ to the discharge. The increased intensity of these emission lines with more oxygen could be due to energy transfer with excited molecular oxygen species or higher gas temperatures in the plasma. No molecular oxygen emission bands were observed in the spectra, which indicates $O_2$* species were not abundant in the discharge and, as a result, are unlikely to be the cause of enhanced He and $N_2$ emission. In contrast, it is well known that gas temperatures of plasmas are higher when a molecular discharge gas is introduced, due to the introduction of vibrational energy levels. In fact, above 0.3% $O_2$ in the FAPA plasma, the cathode became red hot and the discharge appeared to transition towards an arc. Visually, the positive column contracted radially and went from a purple/pink glow to a white filament; all indications of a glow-to-arc transitional discharge. In addition, a plot of the FAPA discharge power as a function of $O_2$ composition (*cf.* Figure S4a) shows a notable change in slope starting at *ca.* 0.15% $O_2$. Transition from a glow to an arc discharge is commonly characterized by a strong negative dynamic resistance. Because the FAPA discharge current was held constant in this case, the negative dynamic resistance of an arc-like discharge is manifested as a decline in the positive

slope of the discharge power (i.e. the derivative of power with respect to gas composition) as is observed in Figure S4a. Therefore, it is likely that the increase in emission intensity for He, O, and $N_2$ at larger $O_2$ fractions is due to a significant shift in the electric field distribution and possibly also the overall increased discharge power (*cf.* Figure S4) as it transitioned from a stable glow discharge to an arc.

It might seem perhaps surprising that $N_2^+$ emission did not exhibit the same trend as other emitting species at higher $O_2$ compositions. However, ionization and excitation in a He FAPA discharge is very non-thermal, particularly for $N_2$ and $N_2^+$,[37, 53] due to the large contributions of charge transfer and Penning ionization. Addition of oxygen gas to this system disrupts some of the non-thermal ionization pathways, which would lower ion densities, including excited $N_2^+$.. In addition, $N_2$ emission did not decrease to the same level as $N_2^+$, OH, and $H_\alpha$ emission. Although the FAPA consists of a non-equilibrium plasma, decrement in $N_2^+$ emission might have shifted the steady state towards $N_2$.

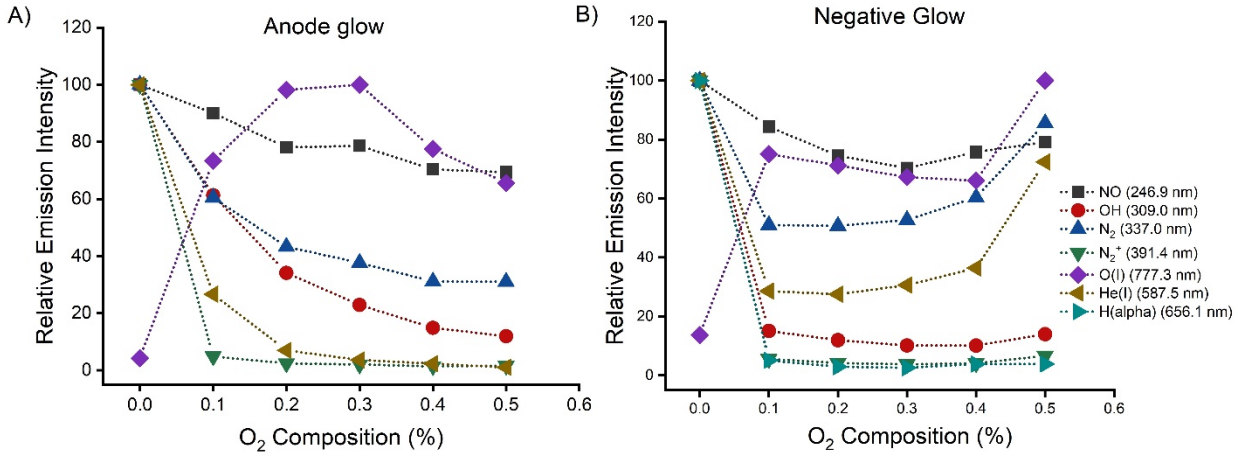


**Figure 7.** Relative emission intensity of NO, OH, $N_2$, $N_2^+$, O, and He from anode and negative glow with respect to $O_2$ composition on He discharge of FAPA source.

Overall, the optical emission results from He:$O_2$ FAPA showed an abrupt change in emission characteristics with 0.1% oxygen and relatively small change with further $O_2$ addition.

These findings corroborate the mass-spectral characterization where the biggest impact on reagent-ion signal was also observed with 0.1% $O_2$ [44].

Gas-kinetic temperature is an important parameter for plasma-based ADI sources as gas temperature plays vital role in desorption of analytes. Approximate gas-kinetic temperature can be obtained by calculating rotational temperatures ($T_{rot}$) from the rovibronic emission of excited OH. Here, the OH rotational temperature was calculated for both the anode and negative glow as a function of $O_2$ composition (*cf.* Figure 8A). It should be noted that the error bars presented in Figure 8 are the associated errors in fitting the slope of the Boltzmann plots. The error bars are results of non-linearity of the data points which could be caused by imperfect transition probability or slight dis-equilibrium in the distribution of the OH rotational levels. Although at first glance, one could conclude that the OH rotational temperatures with gas composition (shown in Figure 8) are statistically insignificant based on the presented errors (only He vs. 1% $N_2$ is statistically significant for $p<0.05$). The observed trends are clear and consistent, particularly for the anode glow, because the changes in temperature appear to be systematic and not random. In the negative glow, the rotational temperature remained approximately constant over the range examined. At the anode glow, the OH rotational temperature increased monotonically with $O_2$ composition. Thiyagarajan *et al.* [54] and Motret *et al.* [55] also observed a rise in rotational temperature with molecular gas composition in helium and argon plasmas. Because of the presence of ro-vibrational levels in a molecule, heat capacities of molecular gases are higher than those of monoatomic gases. The addition of a molecular gas to a glow discharge typically changes the distribution of the electric field (e.g., increasing the field near the cathode) [56, 57]. As such, the measured rotational temperature increases.

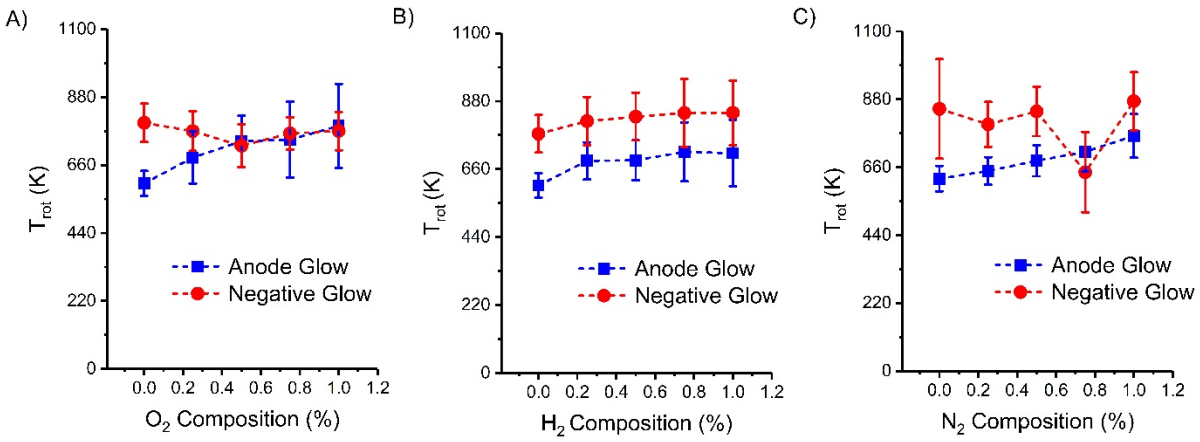


**Figure 8.** OH rotational temperatures estimated from rotational emission band from anode and negative glow with respect to A) $O_2$ composition, B) $H_2$ composition, and C) $N_2$ composition. As a reminder, error bars represent one standard deviation in the temperature determination based on the error in the slope of the fit from the Boltzmann plots.

### 3.5. Optical characterization of He:$H_2$-FAPA

With He:$H_2$-FAPA, a monotonic decrease in He emission intensity was observed in both the negative glow and the anode glow with increasing $H_2$ composition (*cf.* Figure 9). Emission from O and OH decreased by more than 70% when 0.17% $H_2$ was added and declined further with more $H_2$ at both the anode and cathode. In the anode glow, emission from $N_2^+$ decreased by more than ~40% upon $H_2$ addition and declined further with more $H_2$ in the discharge, while it decreased by ~35% on 0.17% and remains approximately same even with further $H_2$ addition.

Hydrogen alpha and beta emission lines both increased by about five-fold in the anode glow when any $H_2$ was added to the discharge. However, the opposite trend for hydrogen atom emission was observed in the negative glow (i.e. a decreased of *ca.* 40%). Currently, the reason for H-emission decrement in the negative glow is not known. With $H_2$ addition, most emission intensity changed significantly with respect to the He-FAPA on 0.17% addition for almost all species and effect was little to none on further addition. The emission data show that addition of $H_2$ quenched excited helium atoms and $N_2^+$. Both of those species are known to be important reactants in the production of protonated water cluster reagent ions. These findings correlate well

with the mass-spectrometric observation of decreased reagent ion signals in the presence of hydrogen (*cf.* Figure 1).

Interestingly, $N_2$ emission increased with $H_2$ composition at both the anode and cathode. The added molecular gas serves as an energy sink for Penning and charge-transfer ionization, a major contributor to the formation and excitation of $N_2^+$ due to the large collision cross sections with excited/ionized helium species.[37, 53] The molecular gas depletes excited helium species and limits direct production of $N_2^{+*}$ from them. Meanwhile, excited $N_2$ production was enhanced relative to $N_2^{+*}$ due to interactions with vibronically excited or ionized $H_2$. These excited/ionized $H_2$-related species would be intermediates in the excitation of $N_2$. In contrast, from an energetic point of view, ionization of $N_2$ from $H_2^+$ is thermodynamically unfavorable.

In fact, this process is at least partially confirmed in the reagent-ion mass spectra where protonated water cluster signal declined by more than three orders of magnitude. In helium plasma ionization sources, $N_2^+$ is a primary reagent in the formation of $[(H_2O)_nH]^+$. So, such a dramatic decline in these reagent ions indicates a major loss in $N_2^+$ formation.

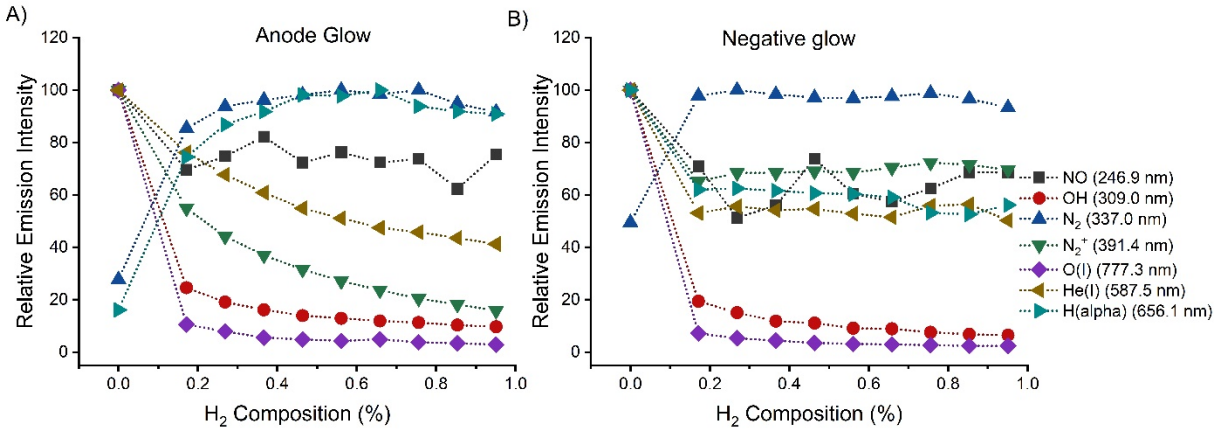


**Figure 9.** Relative emission intensity of NO, OH, $N_2$, $N_2^+$, O, He, and H from anode and negative glow with respect to $H_2$ composition on He discharge of FAPA source.

Addition of $H_2$ to He-FAPA led to a slight increase in the rotational temperature at both the negative and anode glows (*cf.* Figure 8). The monotonic patterns for rotational temperatures in both the anode glow and the negative glow on $H_2$ addition were more consistent compared to $O_2$ or $N_2$ addition. It was also visually observed that the discharge is still quite stable with $H_2$ addition, in contrast to what was observed when $O_2$ was added at 0.3%. Again, the overall slight increment in temperature with $H_2$ addition might be due to availability of vibrational levels to impart energy into.

### 3.6. Optical characterization of He:$N_2$-FAPA

Mass spectrometry data showed that addition of even small fraction (0.2%) of $N_2$ to the He plasma of the FAPA source decreased the reagent-ion signal in the positive-ionization mode. Similar to $H_2$ addition, $N_2$ also quenched the excited helium atoms, but the effect was less dramatic compared to the addition of $O_2$ and $H_2$ (*cf.* Figure 10). Unlike He:$O_2$ and He:$H_2$-FAPA, NO emission increased with $N_2$ addition, which could be related to the enhancement on $NO_3^-$ signal observed with mass spectrometry. To extract a more detailed relationship between these

excited atoms and molecules with the ions observed with mass spectrometer, a thorough computational study is needed [58].

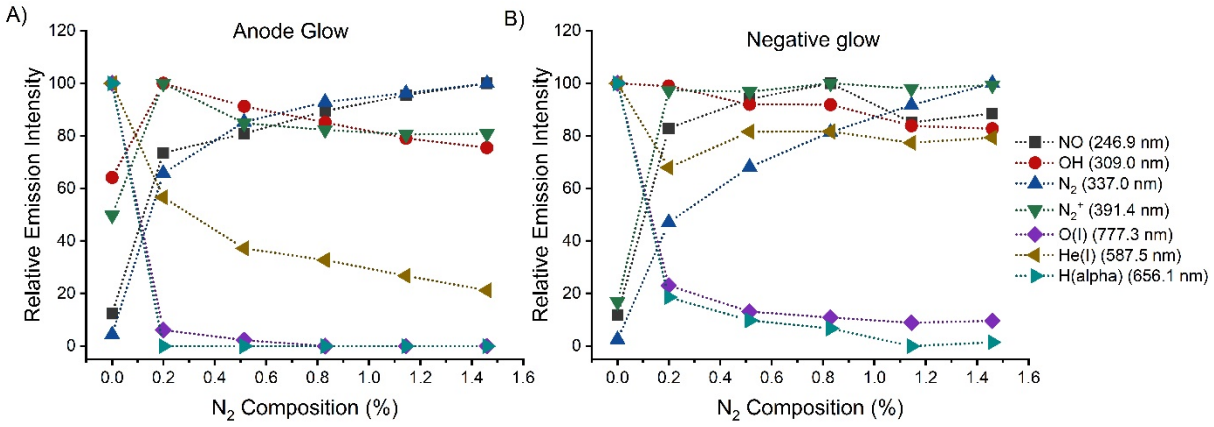


**Figure 10.** Relative emission intensity of NO, OH, $N_2$, $N_2^+$, O, He, and H from anode and negative glow with respect to $N_2$ composition on He discharge of FAPA source.

Rotational temperature of OH slightly increased at both anode and cathode also on addition of $N_2$ and the increment pattern seemed smooth except at negative glow with 0.75% $N_2$ addition. The negative glow at pin cathode is very thin and the glow changes in coverage and uniformity occasionally. The irregular rotational temperature data obtained at 0.75% $N_2$ addition could be due to such change in coverage of negative glow. For the anode glow, OH rotational temperature increased by approximately 190 K, 100 K, and 140 K on addition of 1.00% $O_2$, $H_2$, and $N_2$, respectively.

## 4. Conclusions

Addition of molecular gases to He-FAPA resulted unique plasma chemistries as observed with mass spectrometry. The presence of a small fraction of oxygen in a He-FAPA increased protonated water cluster signal and also produced an enhancement in analyte-ion signal small polar analytes such as acetone and methanol, but, compounds with aromatic rings underwent significant chemical modification to produce pyrylium ions.[44] Addition of hydrogen produced

chemically cleaner mass spectra of the analytes tested albeit at lower total signals. Nitrogen addition increased the $NO_3^-$ ion signal and, correspondingly, $[RDX+NO_3]^-$ was also enhanced in negative-ionization mode. Optical characterization of mixed-gas FAPA suggested that addition of molecular gas to He-FAPA significantly quenches the metastable helium atoms that are mainly responsible for the formation of reagent ions in the afterglow of FAPA. This study sheds light on how presence of molecular gasses on helium plasma of FAPA source affects the plasma processes and ionization chemistries. Addition of molecular gases to a He-FAPA can improve detection capabilities (*e.g.*, increased sensitivity, better S/N, and/or decreased spectral complexity) as well as enable selective analyte detection. However, it is clear that careful control of the gas composition is necessary to reap these benefits as well as maintain a stable glow discharge.

## 5. References


1. Cooks, R.G., et al., *Ambient mass spectrometry.* Science, 2006. **311**(5767): p. 1566-1570.
2. Takats, Z., et al., *Mass spectrometry sampling under ambient conditions with desorption electrospray ionization.* Science, 2004. **306**(5695): p. 471-473.
3. Chernetsova, E.S., et al., *DART mass spectrometry: a fast screening of solid pharmaceuticals for the presence of an active ingredient, as an alternative for IR spectroscopy.* Drug testing and analysis, 2010. **2**(6): p. 292-294.
4. Pavlovich, M.J., B. Musselman, and A.B. Hall, *Direct analysis in real time—Mass spectrometry (DART-MS) in forensic and security applications.* Mass spectrometry reviews, 2018. **37**(2): p. 171-187.
5. Kauppila, T.J., et al., *Rapid analysis of metabolites and drugs of abuse from urine samples by desorption electrospray ionization-mass spectrometry.* Analyst, 2007. **132**(9): p. 868-875.
6. Shelley, J.T., et al., *Ambient desorption/ionization mass spectrometry: evolution from rapid qualitative screening to accurate quantification tool.* Analytical and Bioanalytical Chemistry, 2018: p. 1-16.
7. Wiseman, J.M., et al., *Tissue imaging at atmospheric pressure using desorption electrospray ionization (DESI) mass spectrometry.* Angewandte Chemie International Edition, 2006. **45**(43): p. 7188-7192.
8. Shelley, J.T., S.J. Ray, and G.M. Hieftje, *Laser ablation coupled to a flowing atmospheric pressure afterglow for ambient mass spectral imaging.* Analytical chemistry, 2008. **80**(21): p. 8308-8313.

9. Fowble, K.L., et al., *Development of "Laser Ablation Direct Analysis in Real Time Imaging" Mass Spectrometry: Application to Spatial Distribution Mapping of Metabolites Along the Biosynthetic Cascade Leading to Synthesis of Atropine and Scopolamine in Plant Tissue.* Analytical chemistry, 2017. **89**(6): p. 3421-3429.
10. Cody, R.B., J.A. Laramée, and H.D. Durst, *Versatile new ion source for the analysis of materials in open air under ambient conditions.* Analytical Chemistry, 2005. **77**(8): p. 2297-2302.
11. Monge, M.E., et al., *Mass spectrometry: recent advances in direct open air surface sampling/ionization.* Chemical reviews, 2013. **113**(4): p. 2269-2308.
12. Albert, A., J.T. Shelley, and C. Engelhard, *Plasma-based ambient desorption/ionization mass spectrometry: state-of-the-art in qualitative and quantitative analysis.* Analytical and bioanalytical chemistry, 2014. **406**(25): p. 6111-6127.
13. Dane, A.J. and R.B. Cody, *Selective ionization of melamine in powdered milk by using argon direct analysis in real time (DART) mass spectrometry.* Analyst, 2010. **135**(4): p. 696-699.
14. Gross, J.H., *Direct analysis in real time—a critical review on DART-MS.* Analytical and bioanalytical chemistry, 2014. **406**(1): p. 63-80.
15. Na, N., et al., *Development of a dielectric barrier discharge ion source for ambient mass spectrometry.* Journal of the American Society for Mass Spectrometry, 2007. **18**(10): p. 1859-1862.
16. Harper, J.D., et al., *Low-temperature plasma probe for ambient desorption ionization.* Analytical chemistry, 2008. **80**(23): p. 9097-9104.
17. Andrade, F.J., et al., *Atmospheric pressure chemical ionization source. 1. Ionization of compounds in the gas phase.* Analytical Chemistry, 2008. **80**(8): p. 2646-2653.
18. Andrade, F.J., et al., *Atmospheric pressure chemical ionization source. 2. Desorption− ionization for the direct analysis of solid compounds.* Analytical Chemistry, 2008. **80**(8): p. 2654-2663.
19. Shelley, J.T., J.S. Wiley, and G.M. Hieftje, *Ultrasensitive ambient mass spectrometric analysis with a pin-to-capillary flowing atmospheric-pressure afterglow source.* Analytical Chemistry, 2011. **83**(14): p. 5741-5748.
20. Badal, S.P., et al., *Tunable ionization modes of a flowing atmospheric-pressure afterglow (FAPA) ambient ionization source.* Analytical Chemistry, 2016. **88**(7): p. 3494-3503.
21. Pfeuffer, K.P., et al., *Halo-shaped flowing atmospheric pressure afterglow: a heavenly design for simplified sample introduction and improved ionization in ambient mass spectrometry.* Analytical chemistry, 2013. **85**(15): p. 7512-7518.
22. McEwen, C.N., R.G. McKay, and B.S. Larsen, *Analysis of solids, liquids, and biological tissues using solids probe introduction at atmospheric pressure on commercial LC/MS instruments.* Analytical Chemistry, 2005. **77**(23): p. 7826-7831.
23. Smith, M.J., N.R. Cameron, and J.A. Mosely, *Evaluating atmospheric pressure solids analysis probe (ASAP) mass spectrometry for the analysis of low molecular weight synthetic polymers.* Analyst, 2012. **137**(19): p. 4524-4530.
24. Doué, M., et al., *High throughput identification and quantification of anabolic steroid esters by atmospheric solids analysis probe mass spectrometry for efficient screening of drug preparations.* Analytical chemistry, 2014. **86**(12): p. 5649-5655.

25. Cossoul, E., et al., *Evaluation of atmospheric solid analysis probe ionization coupled to ion mobility mass spectrometry for characterization of poly (ether ether ketone) polymers.* Analytica chimica acta, 2015. **856**: p. 46-53.
26. Wang, S.-Z., et al., *Evaluation of atmospheric solids analysis probe mass spectrometry for the analysis of coal-related model compounds.* Fuel, 2014. **117**: p. 556-563.
27. Ratcliffe, L.V., et al., *Surface Analysis under Ambient Conditions Using Plasma-Assisted Desorption/Ionization Mass Spectrometry.* Analytical Chemistry, 2007. **79**(16): p. 6094-6101.
28. Brewer, T.M. and J.R. Verkouteren, *Atmospheric identification of active ingredients in over-the-counter pharmaceuticals and drugs of abuse by atmospheric pressure glow discharge mass spectrometry (APGD-MS)*. Rapid Communications in Mass Spectrometry, 2011. **25**(17): p. 2407-2417.
29. Wright, J.P., et al., *The effects of added hydrogen on a helium atmospheric-pressure plasma jet ambient desorption/ionization source.* Journal of The American Society for Mass Spectrometry, 2013. **24**(3): p. 335-340.
30. Chan, G.C.Y., et al., *Spectroscopic plasma diagnostics on a low-temperature plasma probe for ambient mass spectrometry.* Journal of Analytical Atomic Spectrometry, 2011. **26**(7): p. 1434-1444.
31. Brandt, S., et al., *Dielectric barrier discharges applied for soft ionization and their mechanism.* Analytica Chimica Acta, 2017. **951**: p. 16-31.
32. Gyr, L., et al., *Characterization of a Nitrogen-Based Dielectric Barrier Discharge Ionization Source for Mass Spectrometry Reveals Factors Important for Soft Ionization.* Analytical Chemistry, 2019. **91**(10): p. 6865-6871.
33. Klute, F.D., et al., *Capillary Dielectric Barrier Discharge: Transition from Soft Ionization to Dissociative Plasma.* Analytical Chemistry, 2016. **88**(9): p. 4701-4705.
34. Schutz, A., et al., *Tuning Soft Ionization Strength for Organic Mass Spectrometry.* Analytical Chemistry, 2016. **88**(10): p. 5538-5541.
35. Shelley, J.T., et al., *Characterization of Direct-Current Atmospheric-Pressure Discharges Useful for Ambient Desorption/Ionization Mass Spectrometry.* Journal of the American Society for Mass Spectrometry, 2009. **20**(5): p. 837-844.
36. Kratzer, J., Z. Mester, and R.E. Sturgeon, *Comparison of dielectric barrier discharge, atmospheric pressure radiofrequency-driven glow discharge and direct analysis in real time sources for ambient mass spectrometry of acetaminophen.* Spectrochimica Acta Part B-Atomic Spectroscopy, 2011. **66**(8): p. 594-603.
37. Chan, G.C.Y., et al., *Elucidation of Reaction Mechanisms Responsible for Afterglow and Reagent-Ion Formation in the Low-Temperature Plasma Probe Ambient Ionization Source.* Analytical Chemistry, 2011. **83**(10): p. 3675-3686.
38. Shelley, J., G. Chan, and G. Hieftje, *Understanding the Flowing Atmospheric-Pressure Afterglow (FAPA) Ambient Ionization Source through Optical Means.* Journal of the American Society for Mass Spectrometry, 2012. **23**(2): p. 407-417.
39. Schuetz, A., et al., *Soft Argon-Propane Dielectric Barrier Discharge Ionization.* Analytical Chemistry, 2018. **90**(5): p. 3537-3542.
40. Ellis, W.C., et al., *The effects of added hydrogen on noble gas discharges used as ambient desorption/ionization sources for mass spectrometry.* Journal of The American Society for Mass Spectrometry, 2016. **27**(9): p. 1539-1549.

41. Heywood, M.S., N. Taylor, and P.B. Farnsworth, *Measurement of helium metastable atom densities in a plasma-based ambient ionization source.* Analytical chemistry, 2011. **83**(17): p. 6493-6499.
42. Hunter, E.P. and S.G. Lias, *Proton Affinity Evaluation*, in *NIST Chemistry WebBook, NIST Standard Reference Database Number 69*, P.J. Linstrom and W.G. Mallard, Editors., National Institute of Standards and Technology: Gaithersburg, MD 20899.
43. Shelley, J.T., G.C.-Y. Chan, and G.M. Hieftje, *Understanding the flowing atmospheric-pressure afterglow (FAPA) ambient ionization source through optical means.* Journal of the American Society for Mass Spectrometry, 2012. **23**(2): p. 407-417.
44. Badal, S.P., et al., *Formation of Pyrylium from Aromatic Systems with a Helium: Oxygen Flowing Atmospheric Pressure Afterglow (FAPA) Plasma Source.* Journal of The American Society for Mass Spectrometry, 2017. **28**(6): p. 1013-1020.
45. Chan, G.C.-Y., et al., *Spectroscopic plasma diagnostics on a low-temperature plasma probe for ambient mass spectrometry.* Journal of Analytical Atomic Spectrometry, 2011. **26**(7): p. 1434-1444.
46. Orejas, J., et al., *Effect of internal and external conditions on ionization processes in the FAPA ambient desorption/ionization source.* Analytical and bioanalytical chemistry, 2014. **406**(29): p. 7511-7521.
47. Ascenzi, D., et al., *Phenol production in benzene/air plasmas at atmospheric pressure. Role of radical and ionic routes.* The Journal of Physical Chemistry A, 2006. **110**(25): p. 7841-7847.
48. Badal, S. and J. Shelley. *295523-Mixed-Gas Direct-Current Atmospheric-Pressure Glow Discharge (DC-APGD) As A Photoionization Source For Mass Spectrometry* . in *Proceedings of the 66th ASMS Conference on Mass Spectrometry and Allied Topics*. 2018. San Diego, CA.
49. Herman, J.A. and A.X.G. Harrison, *Effect of protonation exothermicity on the chemical ionization mass spectra of some alkylbenzenes.* Organic Mass Spectrometry, 1981. **16**(10): p. 423-427.
50. Herman, J.A. and A.G. Harrison, *Effect of reaction exothermicity on the proton transfer chemical ionization mass spectra of isomeric C5 and C6 alkanols.* Canadian Journal of Chemistry, 2011.
51. Dzidic, I., et al., *Comparison of positive ions formed in nickel-63 and corona discharge ion sources using nitrogen, argon, isobutane, ammonia and nitric oxide as reagents in atmospheric pressure ionization mass spectrometry.* Analytical Chemistry, 1976. **48**(12): p. 1763-1768.
52. Irikura, K.K. and R.D. Johnson, *Is NO3 Formed during the Decomposition of Nitramine Explosives?* The Journal of Physical Chemistry A, 2006. **110**(51): p. 13974-13978.
53. Shelley, J.T., G.C.Y. Chan, and G.M. Hieftje, *Understanding the Flowing Atmospheric-Pressure Afterglow (FAPA) Ambient Ionization Source through Optical Means.* Journal of the American Society for Mass Spectrometry, 2012. **23**(2): p. 407-417.
54. Thiyagarajan, M., A. Sarani, and C. Nicula, *Optical emission spectroscopic diagnostics of a non-thermal atmospheric pressure helium-oxygen plasma jet for biomedical applications.* Journal of Applied Physics, 2013. **113**(23): p. 233302.
55. Motret, O., et al., *Rotational temperature measurements in atmospheric pulsed dielectric barrier discharge-gas temperature and molecular fraction effects.* Journal of Physics D: Applied Physics, 2000. **33**(12): p. 1493.

56. von Engel, A., *Ionized Gases*. 1965: Oxford University Press. 325.
57. Astaf'ev, A.M., O.M. Stepanova, and M.E. Pinchuk, *The Influence of Voltage Polarity on the Regime of Atmospheric-Pressure Glow Discharge Operation in Flows of Atomic and Molecular Gases.* Technical Physics Letters, 2019. **45**(12): p. 1270-1272.
58. Murakami, T., et al., *Afterglow chemistry of atmospheric-pressure helium–oxygen plasmas with humid air impurity*. Plasma Sources Science and Technology, 2014. **23**(2): p. 025005.

# Supplemental Information for

# Optical and Mass-Spectral Characterization of Mixed-Gas Flowing Atmospheric-Pressure Afterglow Sources

Sunil P. Badal[1], Paul B. Farnsworth[2], George C.-Y. Chan[3], Brian T. Molnar[1], Jessica R. Hellinger[1], and Jacob T. Shelley[1, *]

[1]Department of Chemistry and Chemical Biology, Rensselaer Polytechnic Institute, Troy, NY 12180

[2]Department of Chemistry and Biochemistry, Brigham Young University, Provo, UT 84602

[3]Lawrence Berkeley National Laboratory, Berkeley, CA 94720

[*] Corresponding author; 110 8th St., Troy, NY 12180 USA; email: shellj@rpi.edu

# Emission Spectra of Mixed-gas FAPA

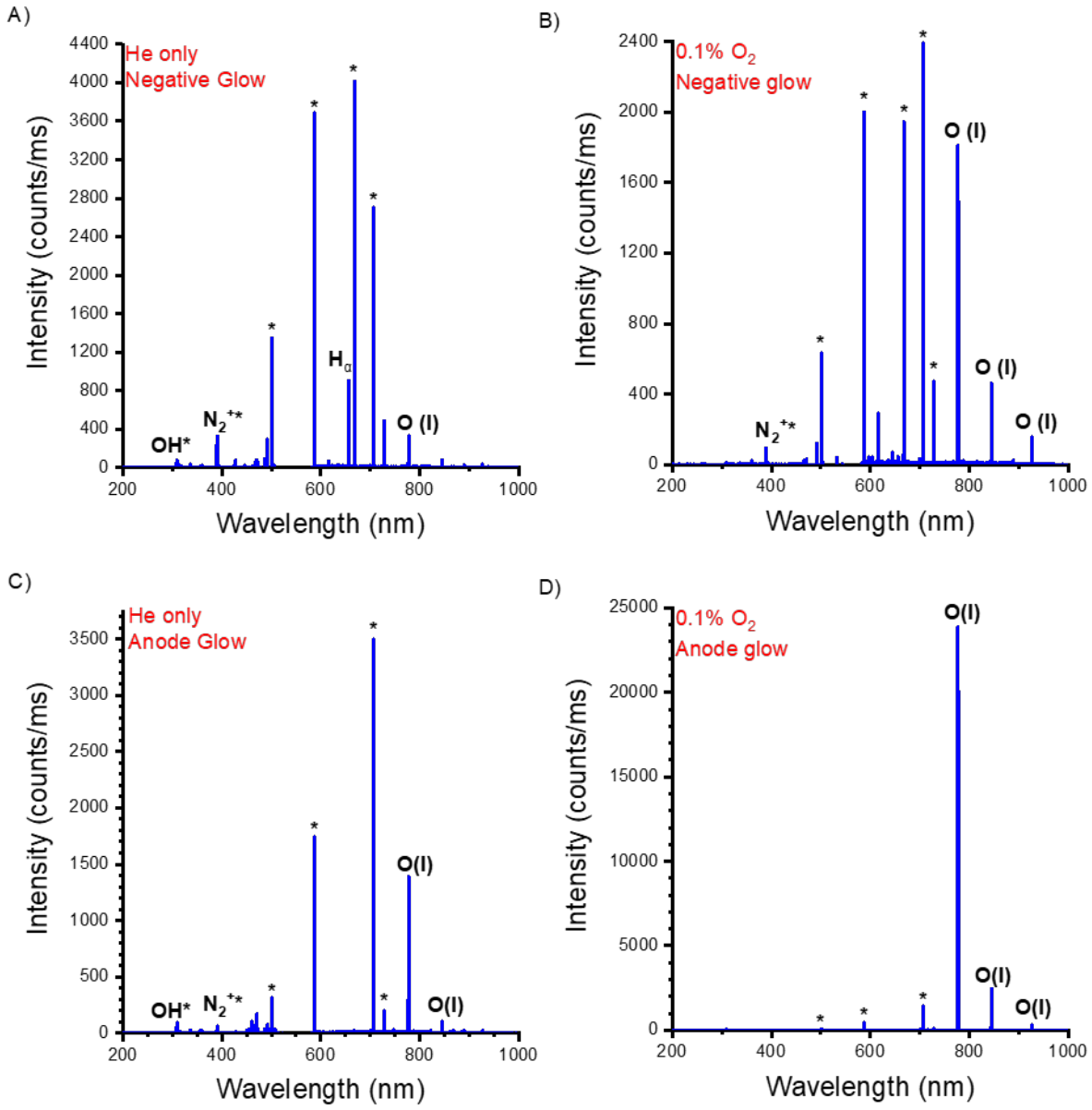


**Figure S1.** Optical emission spectra from the negative-glow (a, b) and anode-glow (c, d) regions of the FAPA source with only helium (a, c) and 0.1% $O_2$ in helium (b, d). Peaks labelled with a star (*) are helium emission lines. Note the significantly different scale in D.

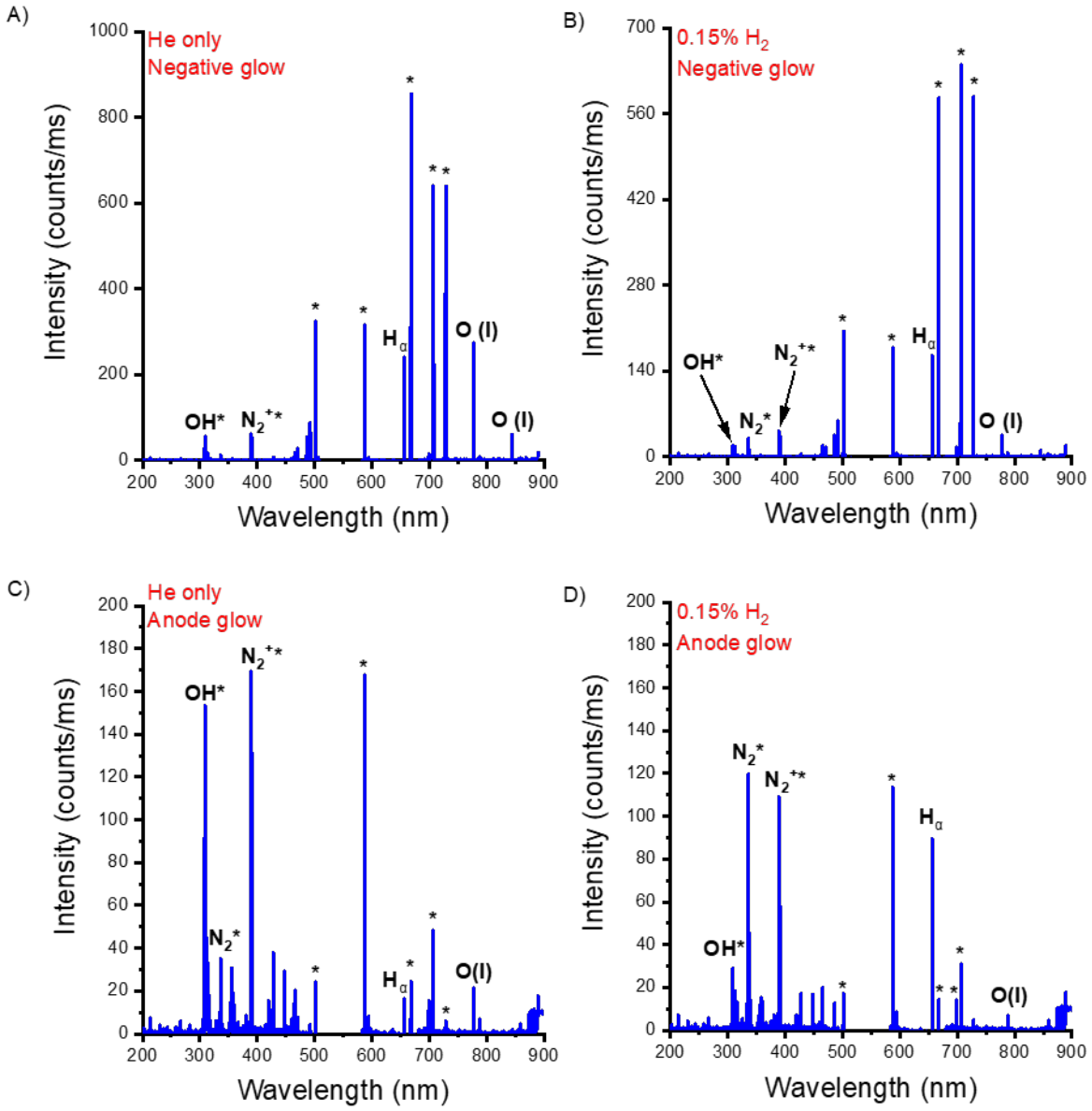


**Figure S2.** Optical emission spectra from the negative-glow (a, b) and anode-glow (c, d) regions of the FAPA source with only helium (a, c) and 0.15% $H_2$ in helium (b, d). Peaks labelled with a star (*) are helium emission lines.

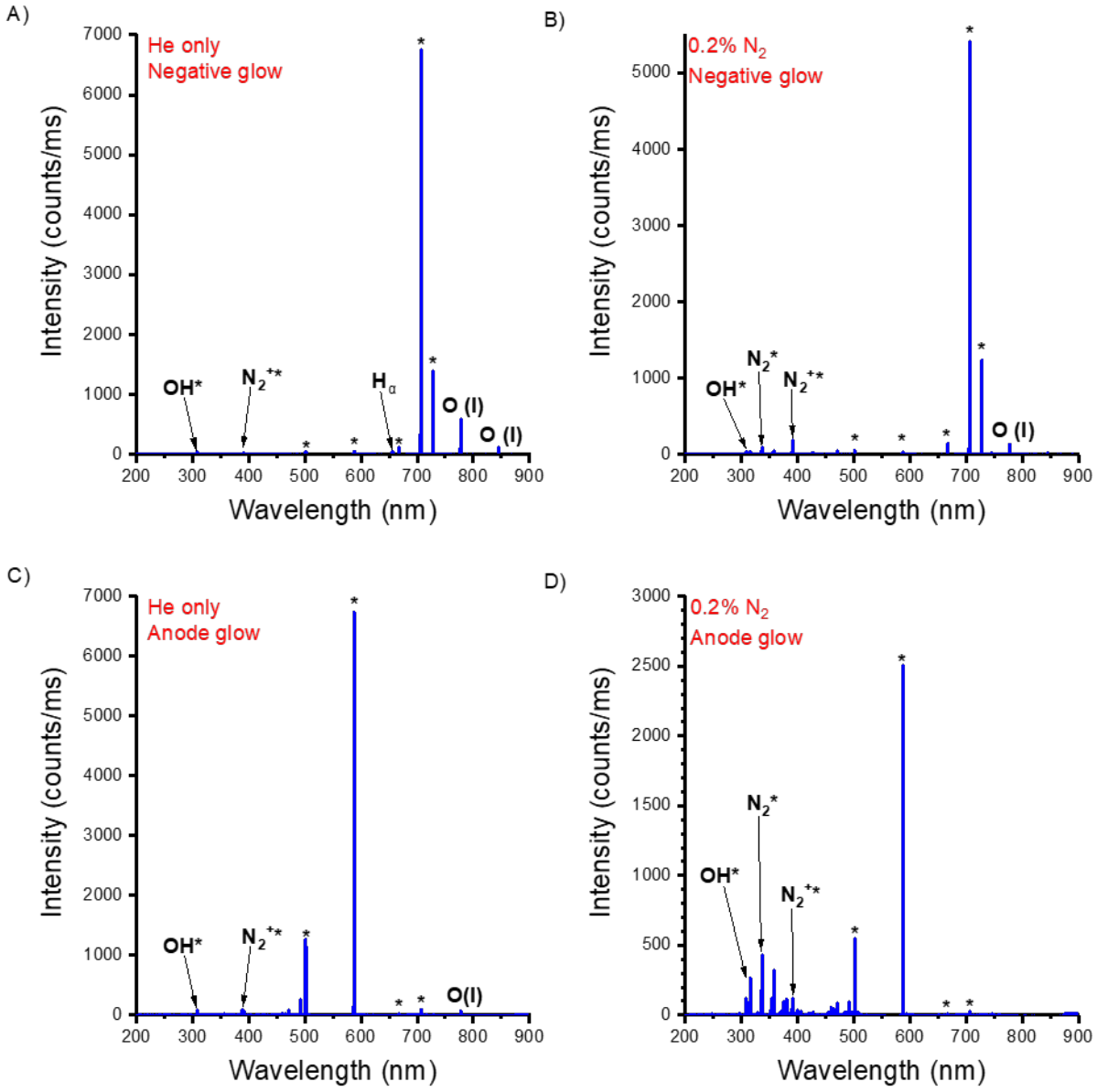


**Figure S3.** Optical emission spectra from the negative-glow (a, b) and anode-glow (c, d) regions of the FAPA source with only helium (a, c) and 0.2% $N_2$ in helium (b, d). Peaks labelled with a star (*) are helium emission lines.

## Discharge Power with Mixed-gas Conditions

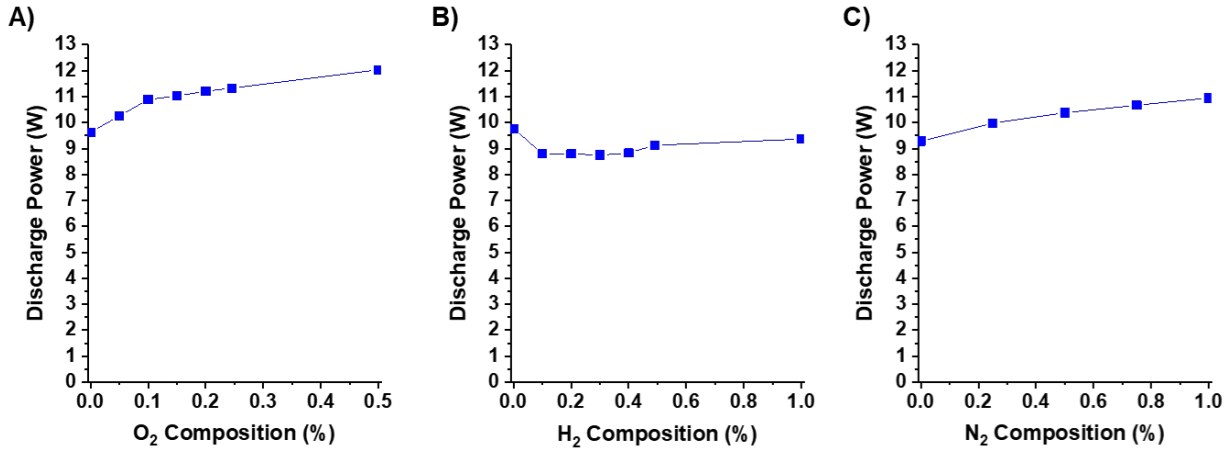


**Figure S4.** FAPA discharge power as a function of percent composition of $O_2$ (A), $H_2$ (B), and $N_2$ (C) at a discharge current of 20 mA. Note that the maximum $O_2$ composition that could be obtained with the flow controllers used was 0.5%.

As can seen above in Figure S2, the FAPA discharge voltage (and power) increased monotonically with $O_2$ and $N_2$ composition. Oxygen addition led to a greater change in discharge power with an increase of 25% when 0.5% $O_2$ was added to the discharge, compared to an 18% power increase for the same amount of $N_2$ in the discharge. Interestingly, addition of $H_2$ to the helium FAPA required lower voltages and powers to sustain the discharge. As $H_2$ composition was elevated above 0.3%, the discharge voltage and power began to rise. The biggest change in discharge voltage and power for $H_2$ addition, compared to only helium, was -10% at an $H_2$ composition of 0.3%.